NEUROSCIENCE

Touch sensation requires the mechanically gated ion channel ELKIN1

Sampurna Chakrabarti[1], Jasmin D. Klich[1], Mohammed A. Khallaf[1,2], Amy J. Hulme[3], Oscar Sánchez-Carranza[1], Zuzanna M. Baran[1,4], Alice Rossi[1], Angela Tzu-Lun Huang[1], Tobias Pohl[4], Raluca Fleischer[1], Carina Fürst[1,5], Annette Hammes[5], Valérie Bégay[1], Hanna Hörnberg[4,6], Rocio K. Finol-Urdaneta[3], Kate Poole[7], Mirella Dottori[3], Gary R. Lewin[1,8,9]*

Touch perception is enabled by mechanically activated ion channels, the opening of which excites cutaneous sensory endings to initiate sensation. In this study, we identify ELKIN1 as an ion channel likely gated by mechanical force, necessary for normal touch sensitivity in mice. Touch insensitivity in *Elkin1*$^{-/-}$ mice was caused by a loss of mechanically activated currents (MA currents) in around half of all sensory neurons activated by light touch (low-threshold mechanoreceptors). Reintroduction of *Elkin1* into sensory neurons from *Elkin1*$^{-/-}$ mice restored MA currents. Additionally, small interfering RNA–mediated knockdown of *ELKIN1* from induced human sensory neurons substantially reduced indentation-induced MA currents, supporting a conserved role for ELKIN1 in human touch. Our data identify ELKIN1 as a core component of touch transduction in mice and potentially in humans.

Touch sensation is fundamental to our sense of self, our social interactions, and our exploration of the tactile world (*1*, *2*). Sensation is initiated at specialized end organs in the skin, innervated by low-threshold mechanoreceptors (LTMRs) with their cell bodies in the dorsal root ganglia (DRGs). The peripheral endings of LTMRs are equipped with mechanically gated ion channels that can be opened by very small forces to initiate and enable touch perception (*3*, *4*). The mechanically gated ion channel PIEZO2 is expressed by most sensory neurons in the DRGs (*5*), and in the absence of PIEZO2, around half of LTMRs no longer respond to mechanical stimuli (*6*–*8*). The DRGs also contain so-called nociceptors, sensory neurons specialized to detect potentially damaging and painful stimuli, including intense mechanical force (*3*). Many nociceptors express PIEZO2 channels but remain mechanosensitive in its absence. The preservation of mechanosensitivity in many LTMRs in the absence of PIEZO2 channels (*6*–*8*) led us to search for other mechanically gated ion channels that could account for PIEZO2-independent sensory mechanotransduction.

[1]Molecular Physiology of Somatic Sensation Laboratory, Max Delbrück Center for Molecular Medicine in the Helmholtz Association (MDC), 13125 Berlin-Buch, Germany. [2]Department of Zoology and Entomology, Faculty of Science, Assiut University, Assiut 71516, Egypt. [3]School of Medical, Indigenous and Health Sciences, Molecular Horizons, University of Wollongong, Wollongong, NSW 2522, Australia. [4]Molecular and Cellular Basis of Behavior, Max Delbrück Center for Molecular Medicine in the Helmholtz Association (MDC), 13125 Berlin-Buch, Germany. [5]Molecular Pathways in Cortical Development, Max Delbrück Center for Molecular Medicine in the Helmholtz Association (MDC), 13125 Berlin-Buch, Germany. [6]NeuroCure Cluster of Excellence, Humboldt-Universität zu Berlin, 10117 Berlin, Germany. [7]School of Biomedical Sciences, Faculty of Medicine & Health, University of New South Wales, Sydney, NSW 2052, Australia. [8]Charité-Universitätsmedizin Berlin, 10117 Berlin, Germany. [9]German Center for Mental Health (DZPG), partner site Berlin, 10117 Berlin, Germany.
*Corresponding author. Email: glewin@mdc-berlin.de

ELKIN1 can detect mechanical force

We previously identified ELKIN1 (TMEM87A) as a protein that is both necessary and sufficient to confer mechanosensitivity to highly metastatic human melanoma cells (*9*). Cryo–electron microscopy (cryo-EM) structures of human ELKIN1 recently revealed a monomeric seven-transmembrane protein with an N-terminal extracellular Golgi-dynamics domain fold (GOLD domain) (*10*). A second, higher-resolution structure recently identified a cation-conduction pathway through the protein (*11*). We overexpressed *Elkin1* in human embryonic kidney (HEK) 293T cells lacking PIEZO1 channels (HEK293T$^{Piezo1-/-}$ cells) (*12*) and found large indentation-induced mechanically activated currents (MA currents) in a majority of transfected cells (Fig. 1, A and B). Cells were plated on laminin 511 and poly-L-lysine (PLL), a substrate that supports increased mechanosensitivity (*13*); untransfected cells showed no indentation-induced currents. ELKIN1-dependent currents were rapidly-adapting (RA) with fast inactivation time constants (<10 ms), similar to those of PIEZO2 ion channels (*5*, *14*) (Fig. 1, A to C). Using substrate deflection by means of pillar arrays (*9*, *14*), we also found robust, mechanically activated currents in all HEK293T$^{Piezo1-/-}$ cells transfected with *Elkin1*-expression constructs, but also in cells transfected with *Elkin1* lacking the N-terminal GOLD-domain (*Elk1Δ170*) (Fig. 1, C and D, and fig. S1A) (*9*). Most of the pillar-evoked currents were RA (inactivation <10 ms) or intermediately adapting [(IA), inactivation between 10 and 50 ms]. Measurements of pillar-gated currents at different holding potentials revealed a linear current-voltage relationship with a reversal potential of 0 mV for both *Elkin1*- and *Elk1Δ170*-transfected cells (Fig. 1E). Therefore, our results suggest that the GOLD domain is not necessary for mechanical activation of ELKIN1. ELKIN1 currents showed a distinctive pharmacological profile, being sensitive to the nonspecific pore blocker Gd^{3+}(30 μM) but barely affected by ruthenium red (30 μM), a compound that completely blocks other mechanosensitive channels, such as PIEZO1 and PIEZO2 (*5*, *15*) (Fig. 1F and fig. S1B). Additionally, in agreement with recent reports (*11*, *15*), we found that cells expressing mouse *Elkin1* display prominent leak currents at very positive (>+60 mV) and very negative potentials (<−100 mV) (Fig. 1G and fig. S1C). ELKIN1 reconstituted into proteoliposomes reportedly show single-channel activity at very positive potentials (*16*). We also found that *Elkin1*-transfected HEK293T$^{Piezo1-/-}$ cells showed currents, which were substantially potentiated by application of mild positive-pressure pulses (20 mm of Hg) applied via the cell-attached pipette (fig. S2, A to C). Therefore, we provide multiple lines of evidence that ELKIN1 is likely an ion channel that can detect mechanical force.

Mouse sensory neurons express ELKIN1

We hypothesized that ELKIN1 could also be involved in mammalian touch sensation. We generated a CRISPR-Cas9–mediated genomic deletion of the mouse *Tmem87a/Elkin1* gene locus spanning sequences coding for transmembrane domains 2 to 6, which includes the proposed ion-conduction pathway (fig. S3A) (*11*). Mice homozygous for the genomic deletion (*Elkin1*$^{-/-}$ mice) were viable and born at the expected Mendelian ratios [wild type (WT), 25.7%; *Elkin1*$^{+/-}$, 46.2%; *Elkin1*$^{-/-}$, 28%; n = 132] (table S2). Single-molecule fluorescent in situ hybridization (smFISH) and immunohistochemistry with an antibody against ELKIN1 showed that *Elkin1*$^{-/-}$ mice were complete null mutants (Fig. 2A). Our validated ELKIN1 antibody revealed that ELKIN1 protein levels appeared to be especially high in sensory neurons of the DRGs. ELKIN1 protein was robustly detected in all subsets of DRG neurons, which is consistent with single-cell expression data from mice, macaques, and humans (*17*–*21*); around 60% of neurons showed high ELKIN1 expression (fig. S3, B and C). Sensory neurons expressing high amounts of ELKIN1 made up 34% of neurofilament heavy chain positive ($NF200^+$) large neurons with myelinated axons. High ELKIN1 expression was also found in 75% of isolectin-B4 positive ($IB4^+$) nonpeptidergic small neurons (*22*) and 45% of small neurons positive for the capsaicin-gated transient receptor potential channel, TRPV1 (fig. S3, B and C). Both of these two neurochemically distinct nociceptor types are reported to be responsive to mechanical force (*23*).

Sensory deficits in *Elkin1*$^{-/-}$ mice

The absence of ELKIN1 did not alter the neurochemical makeup of the sensory ganglia

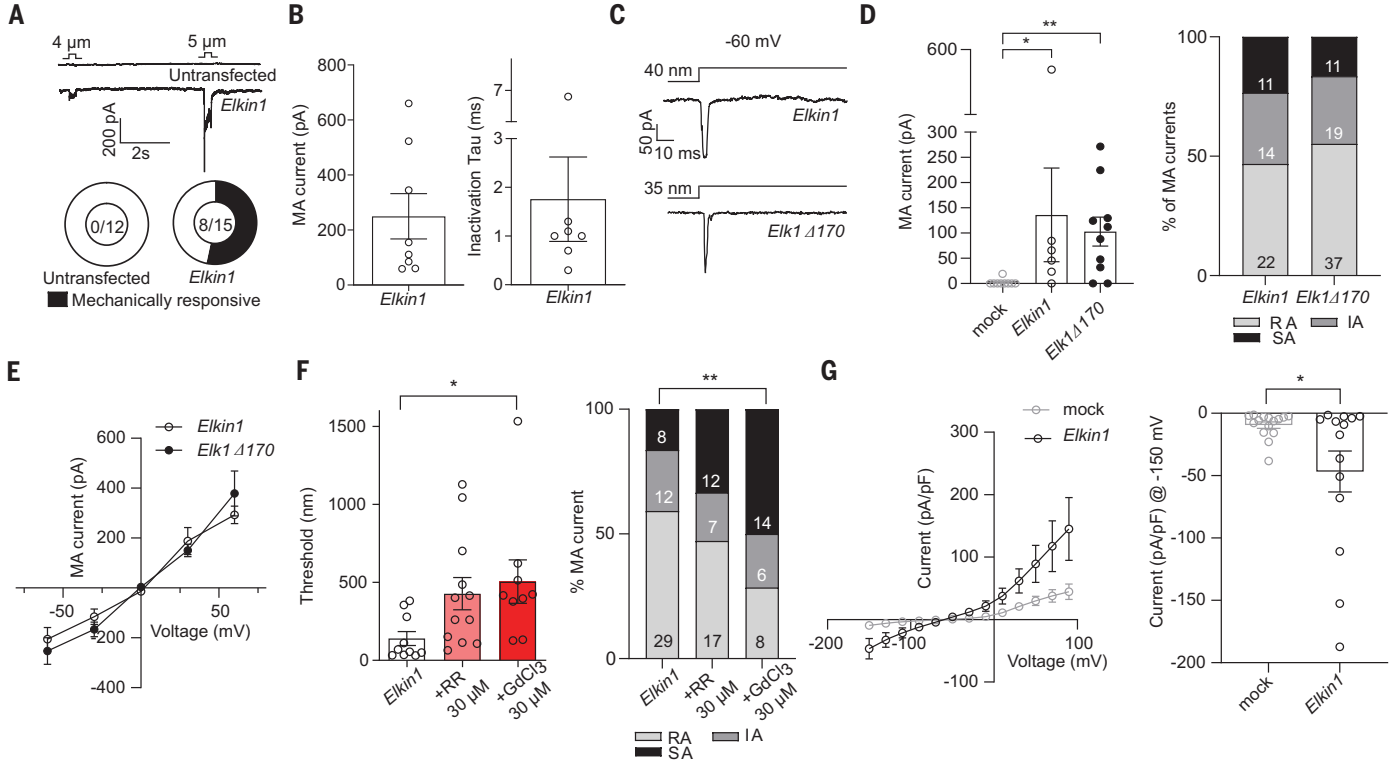

Fig. 1. ELKIN1 forms a mechanically gated channel. (**A**) Pie charts show total number of mechanically responsive transfected cells. Shown in (A) (top) and (**B**) are indentation-induced currents in HEK293T$^{Piezo1-/-}$ cells upon transfection with mouse *Elkin1* cDNA. Dots represent individual cells. (**C**) Representative MA currents evoked by pillar deflection at −60 mV along with (**D**) quantification of MA-current amplitude and properties at 100- to 250-nm force bin (each dot represents a cell, and numbers in bars are number of MA-pillar stimuli). (**E**) Current-voltage relationship of MA currents evoked in cells transfected with *Elkin1* or *Elk1Δ170*. Dots are mean of n = 10 in *Elkin1* and n = 15 in *Elk1Δ170*-transfected cells. (**F**) Quantification of pillar-deflection threshold and properties of ELKIN1-dependent currents in the presence of pore blockers ruthenium red (RR) and $GdCl_3$. Each dot represents a cell, and numbers in bars are number of MA-pillar stimuli. (**G**) Current-voltage relationship of *Elkin1*-transfected cells (each dot is a mean of n = 14 mock and n = 15 *Elkin1* cells) as assessed through a series of voltage steps from −150 to 90 mV. Three group comparisons were made with one-way ANOVA followed by multiple comparison test, and two group comparisons were made with Student's t test. Proportions were compared using χ^2 test. *P < 0.05, **P < 0.01. Error bars indicate SEM.

because the percentage of DRG neurons positive for markers such as NF200, IB4, TRPV1, and tyrosine hydroxylase (TH) was unchanged in the *Elkin1*$^{-/-}$ mice as compared with WT (Fig. 2B). Ultrastructural analysis of the saphenous nerve revealed no pathology or loss of myelinated or unmyelinated axons in *Elkin1*$^{-/-}$ mice (Fig. 2C and table S1). However, behavioral indicators of touch sensitivity, such as percentage of responses to a cotton swab, were profoundly reduced in *Elkin1*$^{-/-}$ mice as compared with WT animals (WT, 90% paw withdrawal versus *Elkin1*$^{-/-}$, 47.5% paw withdrawal; P < 0.0001, unpaired Student's t test) (Fig. 2D). Paw-withdrawal thresholds to von Frey filaments were also significantly elevated [P < 0.0001, two-way analysis of variance (ANOVA) with Sidak post hoc test], with substantial deficits observed across a range of von Frey force filaments in *Elkin1*$^{-/-}$ mice (Fig. 2E). However, responses to brush stimuli in *Elkin1*$^{-/-}$ were similar to those for WT mice (fig. S3E). These results confirm reduced sensitivity to mechanical forces in *Elkin1*$^{-/-}$ mice. However, nonmechanosensory modalities, such as heat withdrawal thresholds, were unaltered in *Elkin1*$^{-/-}$ mice (fig. S3D). *Elkin1*$^{-/-}$ mice also showed no deficits in open-field locomotion (fig. S3E).

Sensory neuron mechanically activated currents are lost in *Elkin1*$^{-/-}$ mice

Large sensory neurons of the DRGs are predominantly mechanoreceptors required for touch (*4*, *24*). We therefore recorded MA currents from isolated sensory neurons evoked by mechanical indentation and substrate deflection (Fig. 3, A and D) (*24*, *25*). Normally, almost all large neurons exhibit robust, predominantly RA MA currents to both cell indentation and substrate deflection (*14*, *25*), which we confirmed in WT animals (Fig. 3, A to F). However, only half of the large neurons (diameter >30 µm, fig. S4A) from *Elkin1*$^{-/-}$ mice displayed any MA current (Fig. 3, B and E). The insensitivity to mechanical stimuli was therefore concomitant to a loss of RA MA currents in *Elkin1*$^{-/-}$ mice (Fig. 3, C and F). The current amplitude of MA currents in the remaining mechanosensitive neurons was similar in WT and *Elkin1*$^{-/-}$ mice; however, there was a small but significant (P = 0.01, unpaired Student's t test) increase in the deflection threshold in neurons from *Elkin1*$^{-/-}$ mice as assessed through the pillar assay (fig. S4, B and C). Large sensory neurons recorded from *Elkin1*$^{-/-}$ mice also showed a slightly depolarized resting membrane potential (P = 0.001, unpaired Student's t test), which is consistent with the idea that this channel may contribute to membrane leak (fig. S4D). A significant loss of MA currents was even detectable after loss of just one *Elkin1* allele (P = 0.005, unpaired Student's t test) (fig. S4E). To show that the loss of MA currents was not due to indirect effects of *Elkin1* gene inactivation, we conducted an acute rescue experiment. Using an adeno-associated virus neurotropic for sensory neurons (AAV-PHP.S-*hSyn-dtomElkin1*), we reintroduced *Elkin1* back into acutely isolated sensory neurons from *Elkin1*$^{-/-}$ mice. ELKIN1 protein was detected in infected sensory neurons from *Elkin1*$^{-/-}$ mice, and there was a significant (P = 0.01, χ^2 test) rescue of MA currents: Only 40% of neurons had MA

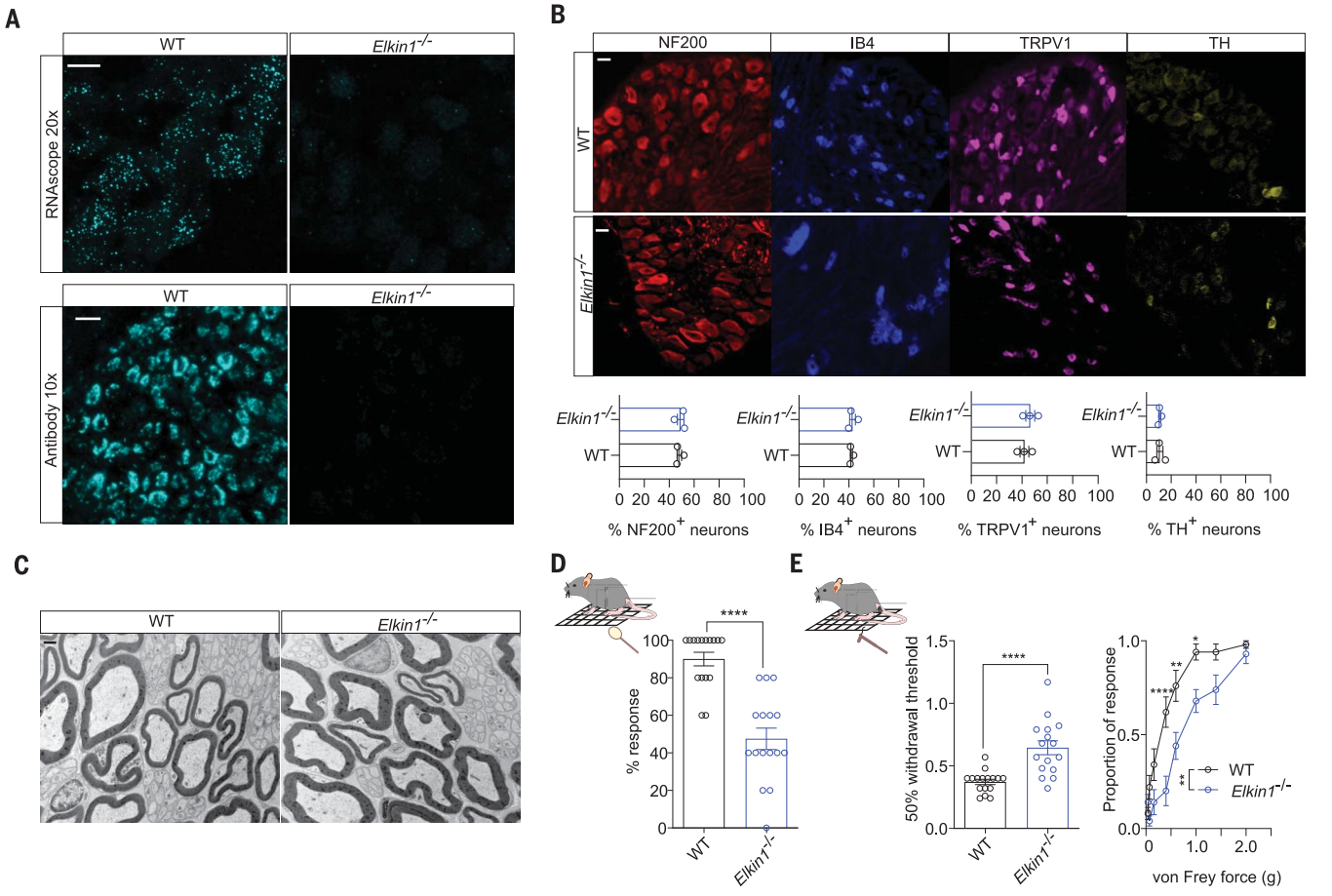

Fig. 2. *Elkin1*$^{-/-}$ mice are touch insensitive. (**A**) Representative images of ELKIN1 expression pattern, obtained using a smFISH probe against *Elkin1* (top panel; scale bar, 20 μm) and antibody staining against ELKIN1 (bottom panel; scale bar, 50 μm) from WT and *Elkin1*$^{-/-}$ DRGs. (**B**) (Top panels) Representative images of NF200 (red), IB4 (blue), TRPV1 (magenta), and TH (yellow) staining in WT and *Elkin1*$^{-/-}$ DRGs and (bottom) quantification of percent of positive neurons in each group from three male mice. More than 500 neurons were counted in each category. (**C**) Ultrastructural analysis of saphenous nerve. Scale bar, 1 μm. (**D**) Percent response of WT and *Elkin1*$^{-/-}$ mice (n = 16) to brushing of a cotton swab. (**E**) Paw withdrawal threshold (left, n = 16) and ascending-dose response (right, n = 10) of WT and *Elkin1*$^{-/-}$ mice to von Frey filaments. Two group comparisons were made with Student's t test and two-way ANOVA with Sidak post hoc test (for von Frey ascending-dose response). $^{**}P < 0.01$, $^{***}P < 0.001$. Error bars indicate SEM. Data from both male and female mice.

currents in mock transfected cells as compared with 75% of cells 48 hours after infection with AAV-PHP.S-*hSyn-dtom-mElkin1* (Fig. 3, G and H, and fig. S5A).

Mechanically activated currents in human sensory neurons depend on *ELKIN1*

Human stem cells can be differentiated into sensory neuron–like cells that have characteristic electrophysiological properties of DRG neurons, including MA currents (*26*, *27*). We could detect ELKIN1 protein in *NEUROGENIN2*-induced human sensory neurons (*26*), the staining for which was abolished by small interfering RNA (siRNA)–mediated mediated knockdown of *ELKIN1* (Fig. 3I and fig. S6A). Our induced human sensory neurons also had robust MA currents, which increased in size with increasing indentation amplitudes. MA currents required higher indentation amplitudes and attained much smaller peak amplitudes in induced sensory neurons transfected with *ELKIN1* siRNA, as compared with control scrambled siRNA (Fig. 3I and fig. S6, B and C). Thus, ELKIN1 is required for normal MA-current expression in both mouse and human sensory neurons. Additionally, in these induced human sensory neurons, knockdown of *PIEZO2* with siRNA also decreased MA currents, and very few MA currents remained after the knockdown of both *ELKIN1* and *PIEZO2* (fig. S6C). We therefore postulated that there may be some functional interaction between PIEZO2 and ELKIN1.

ELKIN1 and PIEZO2 share roles in sensory mechanotransduction

The phenotype that we observed in *Elkin1*$^{-/-}$ sensory neurons was similar to the knockdown or genetic ablation of the PIEZO2 mechanosensitive ion channel (*5*–*7*). Using smFISH, we detected colocalization of *Elkin1* and *Piezo2* mRNA in WT DRG neurons, but no change in *Piezo2* mRNA expression was observed in *Elkin1*$^{-/-}$ sensory neurons (fig. S5B). Thus, *Elkin1* ablation does not affect *Piezo2* expression. As shown previously (*5*), we found that in WT DRG neurons, siRNA-mediated knockdown of *Piezo2* approximately halved the number of neurons with MA currents (fig. S5C). If *Elkin1* exerts its function through *Piezo2*, knockdown of *Piezo2* in *Elkin1*$^{-/-}$ neurons should not cause a further decrease in MA currents. By contrast, our results show that MA currents in *Elkin1*$^{-/-}$ neurons could be reduced further after *Piezo2* knockdown (fig. S5C). Thus, neurons retaining MA currents in *Elkin1*$^{-/-}$ mice appear to have predominantly PIEZO2-dependent MA currents. We next asked whether there is a functional interaction between these two proteins by expressing *Piezo2* or *Piezo2* and *Elkin1* in N2a$^{Piezo1-/-}$ cells. We found no differences in the amplitude or kinetics of MA currents found in single- and double-transfected cells, indicating no substantial functional interaction

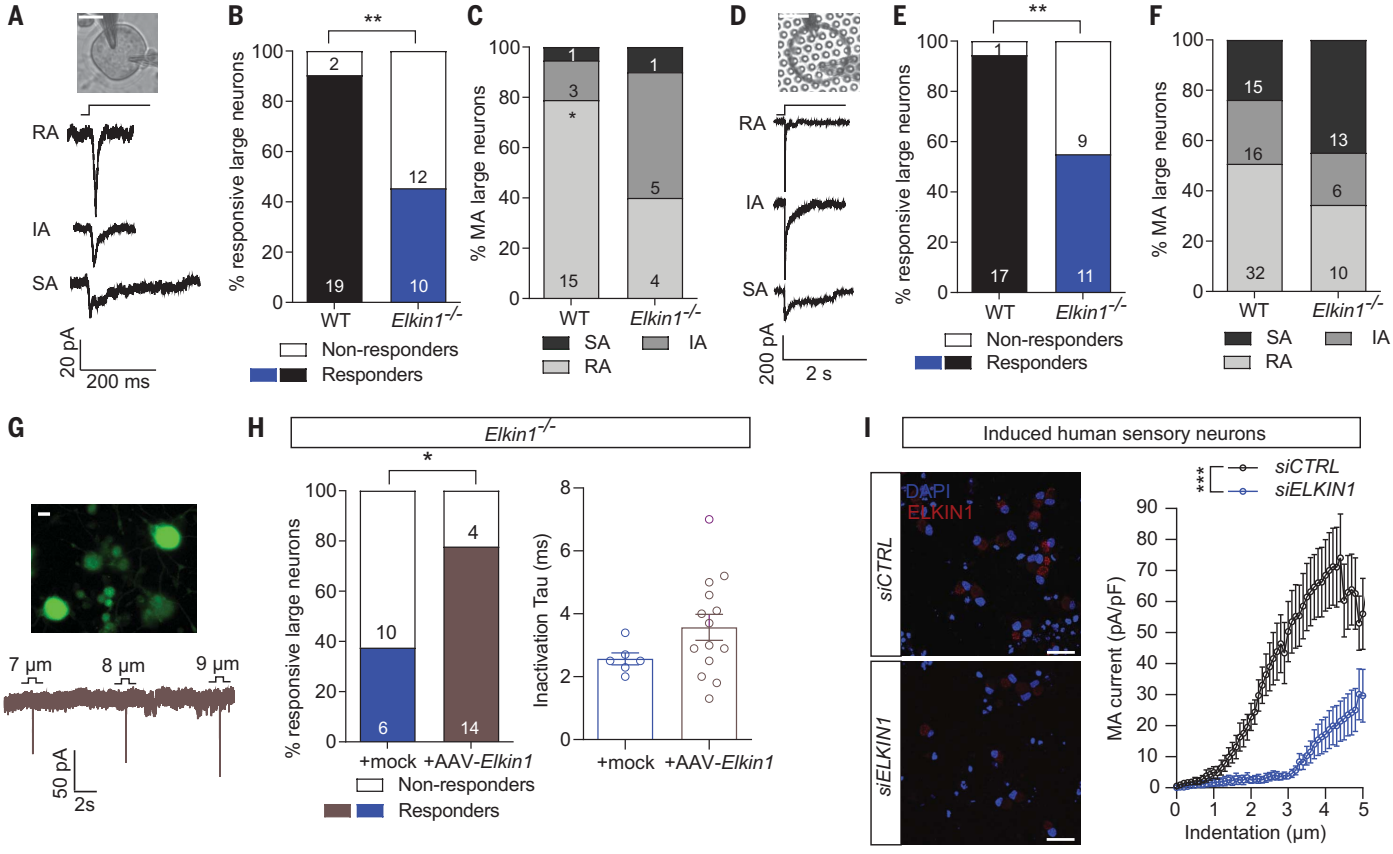

Fig. 3. ELKIN1 is necessary and sufficient for mechanically gated currents in mouse and human sensory neurons. (**A**) Representative traces of currents generated by large-diameter neurons from *Elkin1*$^{-/-}$ mice. Scale bar, 20 µm. (**B**) Percent of large-diameter neurons with an MA current in WT and *Elkin1*$^{-/-}$ mice. (**C**) Percent of rapidly adapting (RA), intermediately adapting (IA), and slowly adapting (SA) MA currents in large-diameter neurons. Number of cells is denoted in the bars. (**D**) Representative traces of currents generated by pillar deflection of a large-diameter neuron from an *Elkin1*$^{-/-}$ mouse. Scale bar, 20 µm. (**E**) Percent of mechanically sensitive large-diameter neurons in WT and *Elkin1*$^{-/-}$ mice in pillar assay. Number of cells is denoted in the bars. (**F**) Percent of RA, IA, and SA MA currents in large-diameter neurons. Number of MA-pillar stimulations is denoted in the bars. (**G**) (Top) Representative image of *Elkin1*$^{-/-}$ DRG neurons stained by anti-RFP after being transduced by AAV-PHP.S-*hSyn-dtom-mElkin1*. Scale bar, 20 µm. (Bottom) Representative traces of indentation-induced currents from a transduced neuron. (**H**) (Left) Percent of mechanically active large-diameter neurons upon transduction with AAV-PHP.S-*hSyn-eGFP* (mock) or AAV-PHP.S-*hSyn-dtom-mElkin1*. (Right) Quantification of inactivation time constants of the measured currents. Each data point represents a single cell measured. (**I**) Representative images of *NEUROGENIN2*-induced human sensory neurons before (top) and after (bottom) transfection with *ELKIN1* siRNA (left, scale bars, 50 µm; right, two-way ANOVA). Proportions were compared using χ^2 test; four group comparisons were made using ANOVA followed by multiple comparison test. *P < 0.05, ** P < 0.01, ***P < 0.001. Error bars indicate SEM. Data from both male and female mice. DAPI, 4′,6-diamidino-2-phenylindole.

between these proteins in a heterologous expression system (fig. S5D).

A known PIEZO2 modulator is the MEC-2–related mechanotransduction protein STOML3, which was shown to sensitize PIEZO2 channels to substrate deflection (*14*, *24*, *28*–*30*). We next asked whether there is also a molecular interaction between STOML3 and ELKIN1. Using a tripartite green fluorescent protein (GFP)–based protein complementation assay, we observed a robust green fluorescent signal, indicating close association between STOML3 and ELKIN1 (fig. S7A). The protein complementation signal for a STOML3/ELKIN1 interaction was also blocked in the presence of the STOML3 oligomerization blocker OB1 (fig. S7A) (*30*). Coexpression of *Stoml3* with *Elkin1* in HEK293T$^{Piezo1-/-}$ cells revealed that ELKIN1-dependent MA currents displayed decreased mechanical thresholds and increased current amplitude in the presence of STOML3 (fig. S7B).

Severe mechanoreceptor deficits in *Elkin1*$^{-/-}$ mice

We next investigated whether ELKIN1 is required for the mechanosensory function of identified mouse mechanoreceptors. First, we used an ex vivo saphenous skin-nerve preparation to trace the trajectory of single units by means of an electrical stimulus until the point of exit from the nerve branch. Using a mechanical stimulus, we then searched for the mechanosensitive receptive field of the same unit, which was usually located close to the exit point from the nerve branch (*6*, *7*, *24*, *31*). Single identified Aβ fibers with the fastest conduction velocities (>10 m/s) usually always have a mechanosensitive receptive field, as confirmed for WT mice (Fig. 4A). However, blinded recordings made from *Elkin1*$^{-/-}$ mice revealed that 40% of the Aβ fibers had no detectable mechanosensitive receptive field (9/26 Aβ fibers) (Fig. 4A). Next, we examined the stimulus-response properties of the remaining identified mechanoreceptors in the hairy skin. Aβ-fiber LTMRs innervating Merkel cells are classified as slowly adapting mechanoreceptors (SAMs) with a dynamic and static response to ramp-and-hold force stimuli (Fig. 4B). Around 50% of Aβ fibers are typically classified as SAMs in the hairy skin (*24*, *32*), and this was the case in both WT and *Elkin1*$^{-/-}$ mice (fig. S8A). However, the firing rates of SAMs to the static constant force phase of the stimulus were strongly reduced at all stimulus strengths in *Elkin1*$^{-/-}$ mice as compared

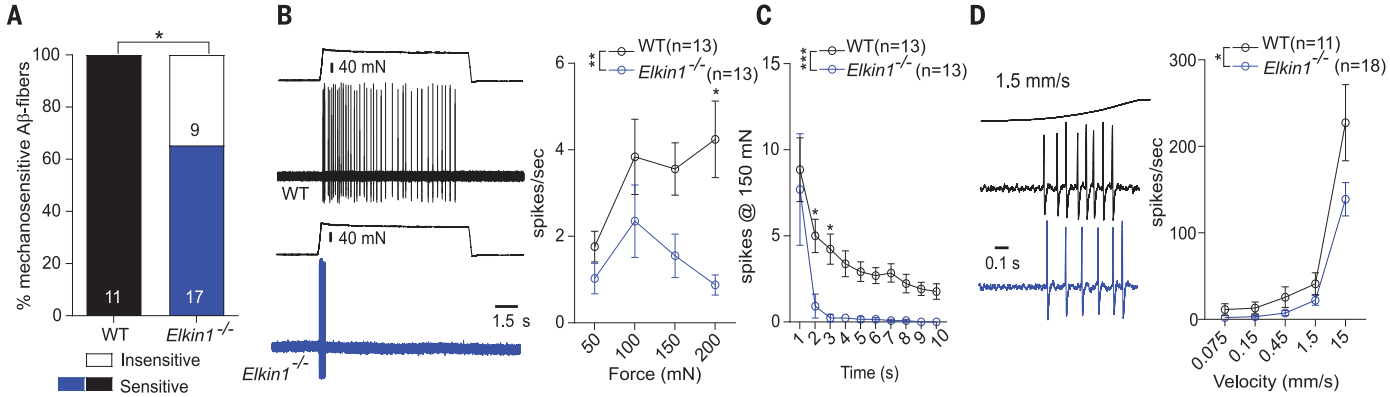

Fig. 4. ELKIN1 is required for LTMR function. (**A**) Percent of mechanosensitive fast-conducting Aβ fibers in the saphenous nerve assessed with an electrical search protocol. (**B**) (Top) Representative spikes evoked from SA mechanosensitive Aβ fibers in WT and *Elkin1*$^{-/-}$ mice and (bottom) quantification of mean spike rates with increasing force. (**C**) Absolute number of spikes over a 10-s time period in the 150-mN force bin (each dot represents average response from fibers). (**D**) Representative spikes evoked from rapidly adapting mechanoreceptors to a moving ramp stimulus and quantification of the mean firing rates to ramps of increasing speed. Proportions were compared using χ^2 test with results from (A). All other group comparisons were made using two-way ANOVA followed by multiple comparison test. *P < 0.05, **P < 0.01, ***P < 0.001. Error bars indicate SEM. Data from both male and female mice.

with those in controls (Fig. 4B). A plot of the peristimulus time histogram for SAMs stimulated with 150 mN of force reveals that firing rates decrease to almost zero just 3 s into a 10-s stimulus (Fig. 4C). However, the same SAMs from WT and *Elkin1*$^{-/-}$ mice showed similar dynamic phase responses (fig S8C). The remaining Aβ mechanoreceptors were classified as rapidly adapting mechanoreceptors (RAMs), which only respond to skin movement and code the velocity of skin movement (*3*, *4*, *33*). As a population, RAMs still coded the velocity of ramp stimuli, but the overall firing rates were significantly lower in *Elkin1*$^{-/-}$ mice as compared with those in controls (P = 0.03, two-way ANOVA with multiple comparison test) (Fig. 4D). These results could easily reflect loss of MA currents in mechanoreceptors but could also be due to morphological disruption of sensory endings. However, an analysis of mechanoreceptor endings in the skin of *Elkin1*$^{-/-}$ mice did not reveal any obvious deficits (fig. S8C). These results show that around half of the LTMRs are insensitive to mechanical forces in *Elkin1*$^{-/-}$ mice, but in addition, the remaining LTMRs showed profound functional deficits in their ability to detect mechanical force.

We also made recordings from single mechanosensitive nociceptors in the saphenous nerve. Sensory neurons with thinly myelinated Aδ axons can be classified as A-fiber mechanonociceptors (AMs), which signal fast pain (*34*), or as down hair (D-hair) receptors, which are specialized LTMRs with directional sensitivity (*35*, *36*). We found no change in the stimulus properties of D-hair or AM afferents in *Elkin1*$^{-/-}$ mice as compared with those of controls (fig. S8D). Many DRGs with high amounts of ELKIN1 also appear to be nociceptors, an assertion based on the presence of markers such as IB4 and TRPV1 (*22*). We thus made a focused analysis of MA currents in small- and medium-diameter neurons that displayed broad-humped action potentials characteristic of nociceptors (*22*, *25*, *37*) (Fig. 5A and fig. S9). Many nociceptors in WT mice lack MA currents to cell indentation (~40%) (*23*, *25*), but this was not different in neurons recorded from *Elkin1*$^{-/-}$ animals (Fig. 5, A and B). However, when the MA currents were classified as RA (inactivation time <10 ms), IA (inactivation time constant 10 to 50 ms), and SA (slowly adapting, inactivation time constant >50 ms), we identified a significant (P = 0.03, χ^2 test) reduction in the proportion of RA MA currents in *Elkin1*$^{-/-}$ mice as compared with those in WT animals (Fig. 5C). In addition, we found a small but significant (P = 0.01, unpaired Student's t test) elevation in the amplitude of indentation needed to evoke the first MA current in nociceptors from *Elkin1*$^{-/-}$ mice (Fig. 5D). MA currents evoked through substrate deflection showed no change between WT and *Elkin1*$^{-/-}$ mice (fig. S9B). We next focused our analysis on nonpolymodal C fibers that respond exclusively to mechanical stimuli and not to thermal stimuli because this population shows robust firing to mechanical force (*38*). In the ramp-and-hold force protocol, the firing of mechanosensitive C fibers from *Elkin1*$^{-/-}$ mice was no different from that in WT animals (Fig. 5, E and F). We next analyzed the time course of C-fiber activation during a 10 s–long constant-force stimulus. C fibers generally show a moderate degree of adaptation during constant-force stimuli (*7*). However, we found that even though initial firing rates were similar between genotypes at a stimulus strength of 100 mN, firing rates dropped significantly more (P = 0.004, two-way ANOVA with multiple comparison test) during the stimulus in C fibers from *Elkin1*$^{-/-}$ mice (Fig. 5, F and G, and fig. S10). Reduced firing rates toward the end of the stimulus were observed for all intensities of stimulation (fig. S10). Thus, unlike in mechanoreceptors, ELKIN1 has a limited role in nociceptors but may be necessary for maintaining sensitivity to constant forces in these neurons.

Discussion

Here we show that ELKIN1 is necessary for the mechanosensory function of most LTMRs. *Elkin1*$^{-/-}$ mice have electrically excitable sensory axons in the skin that were completely unable to respond to mechanical stimuli. The sustained firing of SAMs to constant force partly depends on PIEZO2 expressed in mechanosensory Merkel cells (*39*). Our data suggest that ELKIN1 is required for the PIEZO2 independent transduction in SAMs because sustained responses were severely reduced in *Elkin1*$^{-/-}$ mice. The ability of induced human sensory neurons to transduce mechanical forces was severely diminished after knockdown of *ELKIN1*. Thus, ELKIN1 is an ion channel gated by mechanical force that likely has a conserved role in the transduction of light touch in mice and humans.

Consistent with the expression pattern of ELKIN1, maintained firing of C-fiber nociceptors to constant force was also impaired in the absence of the ELKIN1 protein. The loss of mechanically gated currents, impaired touch-driven behavior, and deficits in LTMR function are reminiscent of mice lacking *Stoml3* and of conditional *Piezo2* mutants (*6*, *7*, *24*, *28*). Our data support a model in which ELKIN1 and PIEZO2 channels share roles in sensory mechanotransduction in LTMRs and in which both channels can be modulated by STOML3. There is evidence that STOML3 can also modulate MA currents in nociceptors, which is consistent

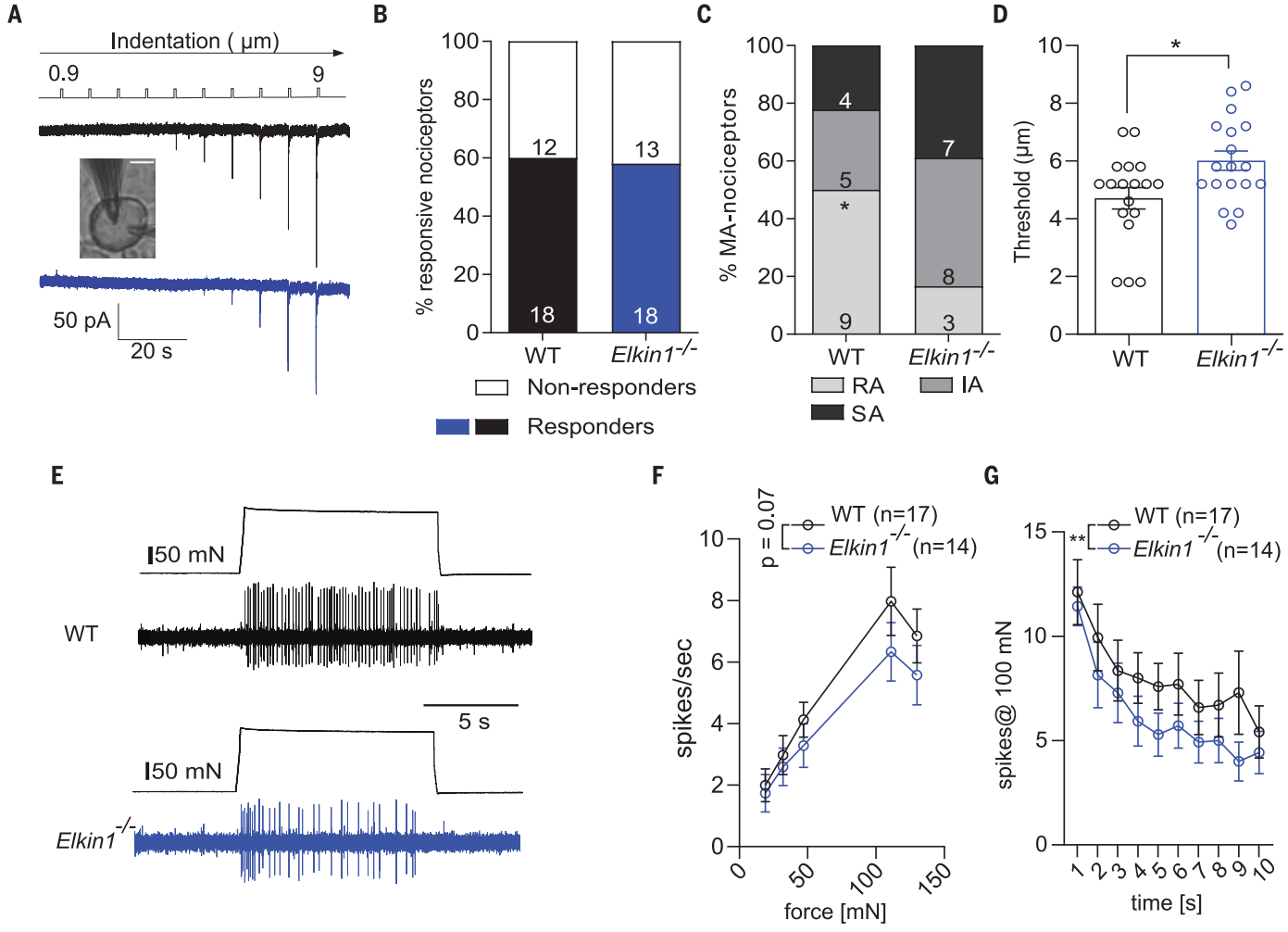

Fig. 5. C mechanonociceptors show reduced firing to sustained mechanical force in *Elkin1*$^{-/-}$ mice. (**A**) Representative indentation-induced current evoked from WT and *Elkin1*$^{-/-}$ small DRG neurons. Scale bar, 20 µm. (**B**) Percent of mechanically sensitive small- and medium-diameter neurons in WT and *Elkin1*$^{-/-}$ mice. (**C**) Percent of RA, IA, and SA MA currents found in small- and medium-diameter neurons and their threshold for activation. (**D**) The number of cells is denoted as dots in the bar graph. (**E**) Representative spikes from mechanosensitive C fibers in WT and *Elkin1*$^{-/-}$ mice. (**F**) Quantification of the firing rates to increasing forces. (**G**) Mean spiking rate over a 10-s time period to a 100-mN force stimulus. Dots in (F) and (G) represent average of all fibers. Proportion was compared using χ^2 test. Two group comparisons were made using Student's *t* test. All other group comparisons were made using two-way ANOVA followed by multiple comparison test. *$P < 0.05$, **$P < 0.01$, ***$P < 0.001$. Error bars indicate SEM. Data from both male and female mice.

with a role for ELKIN1 in conferring robustness to the C-fiber responses to force (*14*). The identification of ELKIN1 as a mechanically gated ion channel necessary for somatosensory function increases our understanding of the entirety of touch transduction.

REFERENCES AND NOTES

1. A. R. Sobinov, S. J. Bensmaia, *Nat. Rev. Neurosci.* **22**, 741–757 (2021).
2. M. Mikkelsen, E. L. Wodka, S. H. Mostofsky, N. A. J. Puts, *Dev. Cogn. Neurosci.* **29**, 140–150 (2018).
3. G. R. Lewin, R. Moshourab, *J. Neurobiol.* **61**, 30–44 (2004).
4. S. G. Lechner, G. R. Lewin, *Physiology* **28**, 142–150 (2013).
5. B. Coste *et al.*, *Science* **330**, 55–60 (2010).
6. S. S. Ranade *et al.*, *Nature* **516**, 121–125 (2014).
7. S. E. Murthy *et al.*, *Sci. Transl. Med.* **10**, eaat9897 (2018).
8. B. U. Hoffman *et al.*, *Proc. Natl. Acad. Sci. U.S.A.* **119**, e2115821119 (2022).
9. A. Patkunarajah *et al.*, *eLife* **9**, e53308 (2020).
10. C. M. Hoel, L. Zhang, S. G. Brohawn, *eLife* **11**, e81704 (2022).
11. A. Han *et al.*, bioRxiv 2023.01.03.522544 [Preprint] (2023). https://doi.org/10.1101/2023.01.03.522544.
12. A. E. Dubin *et al.*, *Neuron* **94**, 266–270.e3 (2017).
13. L.-Y. Chiang *et al.*, *Nat. Neurosci.* **14**, 993–1000 (2011).
14. K. Poole, R. Herget, L. Lapatsina, H.-D. Ngo, G. R. Lewin, *Nat. Commun.* **5**, 3520 (2014).
15. L. Pope, M. Lolicato, D. L. Minor Jr., *Cell Chem. Biol.* **27**, 511–524.e4 (2020).
16. H. Kang *et al.*, bioRxiv 2023.01.03.522543 [Preprint] (2023). https://doi.org/10.1101/2023.01.03.522543.
17. D. Usoskin *et al.*, *Nat. Neurosci.* **18**, 145–153 (2015).
18. N. Sharma *et al.*, *Nature* **577**, 392–398 (2020).
19. J. Kupari *et al.*, *Nat. Commun.* **12**, 1510 (2021).
20. H. Yu *et al.*, bioRxiv 2023.03.17.533207 [Preprint] (2023). https://doi.org/10.1101/2023.03.17.533207.
21. P. Ray *et al.*, *Pain* **159**, 1325–1345 (2018).
22. C. L. Stucky, G. R. Lewin, *J. Neurosci.* **19**, 6497–6505 (1999).
23. L. J. Drew, J. N. Wood, P. Cesare, *J. Neurosci.* **22**, RC228 (2002).
24. C. Wetzel *et al.*, *Nature* **445**, 206–209 (2007).
25. J. Hu, G. R. Lewin, *J. Physiol.* **577**, 815–828 (2006).
26. A. J. Hulme *et al.*, *Front. Cell. Neurosci.* **14**, 600895 (2020).
27. K. Schrenk-Siemens *et al.*, *Nat. Neurosci.* **18**, 10–16 (2015).
28. M. Huang, G. Gu, E. L. Ferguson, M. Chalfie, *Nature* **378**, 292–295 (1995).
29. R. O'Hagan, M. Chalfie, M. B. Goodman, *Nat. Neurosci.* **8**, 43–50 (2005).
30. C. Wetzel *et al.*, *Nat. Neurosci.* **20**, 209–218 (2017).
31. M. Kress, M. Koltzenburg, P. W. Reeh, H. O. Handwerker, *J. Neurophysiol.* **68**, 581–595 (1992).
32. M. Koltzenburg, C. L. Stucky, G. R. Lewin, *J. Neurophysiol.* **78**, 1841–1850 (1997).
33. F. Schwaller *et al.*, *Nat. Neurosci.* **24**, 74–81 (2021).
34. A. Arcourt *et al.*, *Neuron* **93**, 179–193 (2017).
35. J. Walcher *et al.*, *J. Physiol.* **596**, 4995–5016 (2018).
36. M. Rutlin *et al.*, *Cell* **159**, 1640–1651 (2014).
37. H. R. Koerber, R. E. Druzinsky, L. M. Mendell, *J. Neurophysiol.* **60**, 1584–1596 (1988).
38. N. Milenkovic, C. Wetzel, R. Moshourab, G. R. Lewin, *J. Neurophysiol.* **100**, 2771–2783 (2008).
39. S.-H. Woo *et al.*, *Nature* **509**, 622–626 (2014).

40. S. Chakrabarti *et al.*, Touch sensation requires the mechanically gated ion channel ELKIN1, Dryad (2024); https://doi.org/10.5061/dryad.0cfxpnw8s.

ACKNOWLEDGMENTS

We thank F. Bartelt and L. Dalmasso for help with mouse genotyping and B. Purfürst for electron microscopy. We thank J. Poulet, S. Lechner, and members of the Lewin lab for constructive comments on the manuscript. M.D. thanks D. J. Adams for access to the patch-clamp rig. The H9 cell line (WA09) used in this study is available under a material transfer agreement with WiCell. **Funding:** This research was funded by ERC grant Sensational Tethers 789128 and ERA-NET NEURON Sensory Disorders project TRANSMECH to G.R.L., Deutsche Forschungsgemeinshaft grant CRC958 to A.H. and G.R.L., and University of Wollongong, Friedreich's Ataxia Research Alliance (USA), and Friedreich Ataxia Research Association (Australia) to M.D. S.C. and A.R. were recipients of Alexander von Humboldt research fellowships. A.T.-L.H. was a recipient of a Ministry of Science and Technology (Taiwan) fellowship (111-2917-I-564-011). **Author contributions:** Conceptualization: S.C. and G.R.L. Mouse model design and validation: G.R.L. and V.B. Patch clamp physiology and anatomy and cell biology: S.C. with help from O.S.-C., K.P., and Z.M.B. Antibody validation: C.F. and A.H. Human induced sensory neurons and analyses: A.J.H. with help from R.K.F.-U. and M.D. Tripartite-GFP design and implementation: R.F., A.R., and A.T.-L.H. Molecular biology: A.T.-L.H. Skin nerve electrophysiology: J.D.K. (nociceptors), M.A.K. (mechanoreceptors, A-fiber mechanonociceptors, and D-hair receptors), and G.R.L. (electrical search). Behavioral assessment: S.C. with help from T.P. and H.H. Electron microscopy and analysis: J.D.K. and S.C. Writing: S.C. and G.R.L., with input from all authors. Supervision and funding: G.R.L., A.H., and M.D. **Competing interests:** The authors declare that they have no competing interests. **Data and materials availability:** All data are available in the manuscript or the supplementary materials. Prism files are available in Dryad (*40*).

SUPPLEMENTARY MATERIALS

science.org/doi/10.1126/science.adl0495
Materials and Methods
Figs. S1 to S10
Tables S1 and S2
References (*41*–*45*)
MDAR Reproducibility Checklist

Submitted 27 September 2023; accepted 26 January 2024
10.1126/science.adl0495